Received XX Month, XXXX; revised XX Month, XXXX; accepted XX Month, XXXX; Date of publication XX Month, XXXX; date of current version October 17, 2025.

Digital Object Identifier 10.1109/OJVT.XXXX.XXXXXXX

Iterative Soft-MMSE detection aided AFDM and OTFS

HUGO HAWKINS*, GRADUATE STUDENT MEMBER, IEEE, CHAO XU*, SENIOR MEMBER, IEEE, LIE-LIANG YANG*, FELLOW, IEEE, and LAJOS HANZO*, LIFE FELLOW, IEEE

¹School of Electronics and Computer Science, University of Southampton, Southampton SO17 1BJ, UK

CORRESPONDING AUTHOR: Lajos Hanzo (e-mail: lh@ecs.soton.ac.uk).

The financial support of the following Engineering and Physical Sciences Research Council (EPSRC) projects is gratefully acknowledged: Platform for Driving Ultimate Connectivity (TITAN) (EP/X04047X/1; EP/Y037243/1); Robust and Reliable Quantum Computing (RoaRQ, EP/W032635/1); PerCom (EP/X012301/1); India-UK Intelligent Spectrum Innovation ICON UKRI-1859

ABSTRACT Affine Frequency Division Multiplexing (AFDM) has attracted substantial research interest due to its implementational similarity to Orthogonal Frequency-Division Multiplexing (OFDM), whilst attaining comparable performance to Orthogonal Time Frequency Space (OTFS). Hence, we embark on an in-depth performance characterisation of coded AFDM and of its equivalent OTFS counterpart. Soft-Minimum Mean Square Error (MMSE) reception taking into account a priori probabilities in the weighting matrix is applied in conjunction with Recursive Systematic Convolutional (RSC)- and RSC-Unity Rate Convolutional (URC) coding to AFDM. Iterative decoding convergence analysis is carried out with the aid of the powerful semi-analytical tool of EXtrinsic Information Transfer (EXIT) chart, and its Bit Error Rate (BER) performance is compared to OFDM and to the equivalent OTFS configurations. As there are no consistent configurations of AFDM and OTFS utilised in the literature to compare their relative performances, two AFDM configurations and three OTFS configurations are considered. The results show that the BER of AFDM is lower than that of the equivalent OTFS configurations at high Energy per bit over Noise power (E_b/N_0) for small system matrix dimensions, for a low number of iterations, and for high code rates. In all other cases, the BER of AFDM is shown to be similar to that of its equivalent OTFS configurations. Given that the RSC BER performance fails to improve beyond two iterations, this solution is recommended for low-complexity transceivers. By contrast, if the extra complexity of the RSC-URC aided transceiver is affordable, an extra E_b/N_0 gain of 1.8 dB may be attained at a BER of 10^{-5} and a code rate of 0.5.

INDEX TERMS Affine Frequency Division Multiplexing, Orthogonal Frequency-Division Multiplexing, Orthogonal Time Frequency Space, Recursive Systematic Convolutional Codes, Soft-Minimum Mean Square Error, Unity Rate Convolutional codes

I. State-of-the-Art, Motivation, and Contributions

FFINE Frequency Division Multiplexing (AFDM) is a novel chirp-based waveform [1], and it may be deemed reminiscent of Orthogonal Frequency-Division Multiplexing (OFDM), where the Discrete Fourier Transform (DFT) is replaced by the Discrete Affine Fourier Transform (DAFT). The DAFT is a generalised transform, with the DFT being a specific form of the DAFT. It is characterised by two chirp parameters, namely chirp parameter 1 (c_1) and chirp parameter 2 (c_2) , which can be flexibly tuned for optimising the

diversity and correlation properties of the signal. Other forms of OFDM utilising the DAFT [2] or chirps [3], [4] have been proposed, but these still lead to propagation paths being separable only by delay, not Doppler shift. By contrast, the DAFT utilised in AFDM is specifically configured to ensure that the propagation paths are separable by both delay and Doppler shift, similar to Orthogonal Time Frequency Space (OTFS) schemes [5], [6]. This allows AFDM to achieve full diversity, like OTFS. The communication performance of AFDM has also been shown to be similar to that of

1

OTFS [1]. However, the maximum Doppler shift must be known at the transmitter to configure the DAFT. AFDM also requires a prefix to be added, the Chirp Periodic Prefix (CPP), similarly to the OFDM Cyclic Prefix (CP). The CPP reduces to a CP if the value of c_1 for the DAFT meets certain conditions. The correct configuration of the DAFT allows the Affine Frequency Domain (AFD) channel matrix to be sparse, similar to the OTFS Delay-Doppler Domain (DD) channel matrix, but with a different structure.

The similarities between OFDM and AFDM have led to research in many areas of communication [7], such as satellite communication [8], secure transmission [9], [10], and DFT-based AFDM [11]. The DFT-based AFDM may be viewed as a precoded OFDM scheme, to align its implementation more closely to that of OFDM [11].

A. Spectral Efficiency

AFDM has been shown to possess a higher spectral efficiency than OTFS when conventional pilot symbol-based channel estimation is employed [12]–[14]. This is due to the lower number of guard symbols required by AFDM compared to OTFS, as AFDM is a single-domain waveform, whereas OTFS requires guard symbols along both the delay and Doppler domains. However, this spectral efficiency improvement is not seen when other pilot methods are harnessed [15], [16]. For example, when superimposed pilot symbols are considered, this spectral efficiency improvement is no longer observed [15], but superimposed symbols require more complex detection methods for mitigating the interference between pilot and data symbols.

B. Peak to Average Power Ratio

As a drawback, AFDM suffers from high Peak to Average Power Ratio (PAPR), as its structure is similar to OFDM, but it can be reduced by adjusting c_2 of the DAFT [17]. This creates a DAFT with multiple groups of c_2 values within the transform. The authors show that increasing the number of chirp parameter groups decreases the PAPR. This variability in the transmit DAFT leads to a higher Bit Error Rate (BER), when the receiver does not know which c_2 values have been employed. Reddy *et al.* [18] propose to reduce the PAPR by applying μ -law companding and decompanding in the Time Domain (TD), prior to transmission and after reception respectively. This μ -law companding reduces the PAPR of AFDM to a greater extent than the method in [17], with no substantial impact on the BER for moderate companding.

C. Index Modulation

As for OTFS and OFDM, there has also been keen interest in the combination of AFDM and Index Modulation (IM) [19]–[23]. Standard IM applied to AFDM has been shown to slightly reduce the BER of AFDM [19] for both coded and uncoded transmission. This combination has been extended to a multi-antenna scenario in [20], where the transmission from each antenna is shifted by a fixed delay. The addition

of IM is shown to reduce the BER of AFDM in this scenario, albeit at the expense of additional complexity. As expected, the BER of the cyclic transmission method decreases as the number of transmit antennas is increased.

Applying IM to the DAFT parameters has also been proposed [21]. The values of c_2 within groups are varied based on the input bits, in a similar manner to standard IM. This method is shown to result in a lower BER than standard AFDM-IM for Maximum Likelihood (ML) detection. Another innovative IM scheme relies on Walsh-Hadamard sequence based spreading [22]. This is applied on a pergroup basis of chirp subcarriers, and it is shown to lead to a lower BER than both AFDM and standard AFDM-IM for a given throughput at sufficiently high Signal to Noise Ratios (SNRs).

D. Sparse Code Multiple Access

The employment of spreading sequences has also been investigated in multi-user communication. Multi-user Sparse Code Multiple Access (SCMA) aided AFDM is proposed in [24], for both uplink and downlink communications. The authors develop a SCMA codebook design to simplify the input-output relationship in the AFD, thereby allowing for a simpler receiver. The detector proposed for coded transmission iterates between a linear Minimum Mean Square Error (MMSE) receiver and a Low-Density Parity-Check (LDPC) decoder, whose performance is enhanced by the addition of orthogonal approximate message passing. The uncoded and coded AFDM-SCMA schemes are shown to consistently outperform the equivalent OFDM schemes in both uplink and downlink transmission. The equivalent OTFS schemes are shown to have a similar performance to their AFDM counterparts.

E. Integrated Sensing and Communication

As Integrated Sensing and Communication (ISAC) is a subject that attracts considerable interest, research into the employment of AFDM in this field is also ongoing [25]–[33]. An overview and comparison of various waveforms, including OTFS and AFDM, is presented in [25], for various key ISAC performance indicators. The authors show that AFDM inherits a variety of OFDM and OTFS characteristics in communication scenarios. Furthermore, diverse sensing characteristics may be attained due to the flexibility offered by tuning the values of the DAFT chirp parameters.

Ni et al. [26] consider monostatic AFDM ISAC. Multiple AFDM frames are transmitted and received, to produce a received signal matrix, in a similar manner to symbol cancellation-based OFDM ISAC [34]. A pair of detection algorithms are implemented. The first uses the TD signals, and utilises a method similar to symbol cancellation-based OFDM sensing. The second method processes the received Affine Frequency Domain (AFD) signal. The AFD method is shown to experience only small image SNR fluctuations as the Doppler shift is increased. By contrast, the image SNR

of the TD and symbol cancellation-based OFDM methods degrades significantly as the Doppler shift is increased. The AFD method has a higher maximum unambiguous Doppler shift than the TD method, and it is therefore capable of correctly estimating much higher velocities than the TD method. No comparison to OTFS sensing is presented.

Pilot symbol-based monostatic AFDM ISAC is considered in [27], where the pilot symbol is inserted into the transmit signal, with guard bands surrounding it to prevent interference between the pilot and data symbols, as in [12], [13]. Sensing is performed using the guard band and pilot symbol only. This allows for the low-complexity removal of the self-interference imposed by the transmitter on the receiver. This pilot-based sensing method is shown to reach the sensing error floor at a higher SNR than a full signal sensing method, but at a much lower complexity. The performance of AFDM pilot sensing is shown to be comparable to that of OTFS sensing, but the latter employs a more complex interference cancellation method.

Both a monostatic method and a bistatic method are presented in [29], for AFDM, OFDM, and OTFS, utilising probabilistic data association-based message passing and parametric bilinear Gaussian belief propagation, respectively. The performance of AFDM is shown to be similar to that of OTFS, but exhibiting a slightly lower BER and channel parameter MMSE at higher SNRs.

Xiao et al. [30] develop an AFDM sensing method relying on prior knowledge of the channel's delay profile, when assuming that the number of resolvable paths as well as the relative delays between resolvable paths are known, and that there is a single target. This information is leveraged to estimate the target parameters under the assumption that their statistical distributions follow a Nakagami-m distribution. The proposed method is shown to leverage Non-Line of Sight (NLoS) path information, leading to a reduced estimation error, and to an increased robustness to incorrect information. Nonetheless, the performance of the proposed method is more vulnerable to degradation caused by increases in target velocity than the benchmark algorithm.

A super-imposed pilot based method is proposed in [31] for AFDM monostatic ISAC and bistatic channel estimation. Channel estimation is performed by an MMSE algorithm, whilst target parameter estimation is achieved by implementing a TD compensation-based correlation method. The pilot symbols used are Zadoff-Chu sequences. The results presented show that the proposed system is capable of outperforming other pilot-based channel estimation methods, including the method of [15]. In contrast to [15], the proposed pilot arrangement performance does not significantly deteriorate when large delays are present. The pilot arrangement of [31] also leads to a lower incorrect detection probability than that of [15]. No comparison is offered to illustrate the target parameter estimation error performance.

F. Iterative Equalisation and Channel Coding

Due to the relative novelty of AFDM, there is a paucity of publications investigating the benefits of iterative equalisation and channel coding on the performance of AFDM. Nonetheless, a low complexity iterative linear-MMSE-based equalisation method is proposed for AFDM in [35]. The authors first determine the optimum DAFT chirp parameter values to minimise the BER when MMSE equalisation is employed. An iterative TD MMSE method is developed to reduce the complexity of soft linear-MMSE detection. The authors show that the proposed chirp parameter selection method allows the system to reach the BER lower bound. This advantage becomes more apparent when the propagation channel is doubly selective. The proposed iterative TD MMSE method is shown to have a slightly higher BER than iterative linear-MMSE. The performances of AFDM and OTFS are similar to each other for both equalisation methods. Soft-MMSE has also been utilised to improve the BER performance of AFDM in wideband channels [36].

Channel coding has also been investigated in [19], [37]. Xu et al. [37] develop a multi-block unitary transform-based approximate message passing algorithm for AFDM under fractional delay and Doppler indices. Fractional delay indices are scarcely covered in the AFDM literature. This algorithm is conceived to mitigate the energy dispersion effects of the fractional channel indices on the received signal. The proposed algorithm is shown to exhibit a higher iterative gain, illustrated by "empirical" EXtrinsic Information Transfer (EXIT) chart analysis, and a lower BER than the Gaussian approximate message passing benchmark. This algorithm also allows AFDM to exhibit a lower BER than OTFS, since AFDM only experiences interference in a single dimension, as opposed to two dimensions for OTFS. Channel coding was not the focus of the contributions of [19] and [37].

The only currently published work that considers the combination of iterative equalisation and channel coding for AFDM communication is [24]. The soft-MMSE method implemented is specifically designed for SCMA, and hence is not generally applicable to AFDM systems.

G. Motivation and Contributions

As discussed above, AFDM has attracted substantial interest due to its similarity in implementation to OFDM, whilst allowing for comparable performance to OTFS. Although some publications consider coded AFDM and soft-MMSE, there is no in-depth comparison of coded AFDM to its equivalent OTFS counterpart. Hence, the current work addresses this knowledge gap. Table 1 boldly contrasts the novelties of the proposed system to the existing literature. The specific contributions of this work are detailed below:

• Firstly, a parametric study of the communication performance of OFDM, AFDM and OTFS in doubly selective fading is performed for both coded and uncoded transmission. Multiple OTFS and AFDM configurations, defined in Table 2, are investigated, since the existing

TABLE 1: Comparison of contributions from the literature

Papers Topics	[13]	[19]	[20]	[24]	[29]	[35]	[37]	This work
System overview								
Doubly selective channel	√	√	✓	✓	✓	✓	√	✓
Channel coding		√		√			√	✓
Comparison between AFDM, OTFS and OFDM	✓			√	√	✓	√	✓
Receive signal processing		•			•			
Iterative detection			✓	√	✓	✓	√	✓
Soft-MMSE				√		✓		✓
URC code assisted decoding								✓
Iterative soft-MMSE and RSC decoding								✓
Performance analysis								
EXIT chart and trajectory analysis							√	✓
Scalable numerology for AFDM and OTFS configurations		√	✓					✓
Respective application domains of AFDM and OTFS configurations are								✓
identified								

TABLE 2: OFDM, OTFS and AFDM configurations

	OFDM	AFDM 1	OTFS 1	AFDM 2	OTFS 2	OTFS 3
Dimension	M	$\ddot{N}_1 = MN$	MN	M	$M_2N_2 = M$	MN
Subcarrier	Δf	$\Delta f_1 = \frac{\Delta f}{N}$	Δf	Δf	$\Delta f_2 = N_2 \Delta f$	Δf_1
spacing						
Bandwidth	$M\Delta f$	$\ddot{N}_1 \Delta f_1 = M \Delta f$	$M\Delta f$	$M\Delta f$	$M_2 \Delta f_2 = M \Delta f$	$M\Delta f_1 = \frac{M\Delta f}{N}$
Duration	T	$\frac{1}{\Delta f_1} = NT$	NT	T	$\frac{N_2}{\Delta f_2} = T$	$\frac{N}{\Delta f_1} = N^2 T$
Delay resolution	$\frac{\frac{1}{M\Delta f}}{\frac{\Delta f}{N}}$	$\frac{1}{M\Delta f}$	$\frac{1}{M\Delta f}$	$\frac{1}{M\Delta f}$	$\frac{1}{M\Delta f}$	$rac{N}{M\Delta f}$
Doppler	$\frac{\Delta f}{N}$	$\frac{\overline{M\Delta f}}{\overline{M}}$	$\frac{\overline{M}\Delta f}{\overline{M}}$	Δf	Δf	$\frac{\Delta f}{N^2}$
resolution						
Throughput	B_S	B_S	B_S	B_S	B_S	$\frac{B_S}{N}$
Complexity per	M	MN	MN	M	M	MN
block						
References	[8], [18], [19],	[1], [10],	[1], [7],	[7], [8], [11],	[20]	[10], [24], [37]
	[21], [26]	[12]–[15], [20],	[11]–[15], [28],	[18], [19], [21],		
		[28], [32],	[32], [35], [36]	[26]		
		[35]–[37]				

publications tend to compare AFDM to OTFS with different subcarrier spacings and/or bandwidths [10], [13], [20]. OTFS 1 is the original OTFS configuration of [5], [6] whose subcarrier spacing and number of subcarriers are identical to OFDM. The AFDM 1 scheme of [1], [12], [13] is equivalent to OTFS 1, where both schemes share the same matrix dimension. Furthermore, OTFS 2 [20] and AFDM 2 [15], [32], [35] have the same matrix dimension as a single OFDM symbol. These five configurations utilise the same bandwidth. The last configuration, OTFS 3 [10], [24], [37], has the same matrix dimension as OTFS 1, but its subcarrier spacing is identical to that of AFDM 1.

• Secondly, a soft-MMSE equalisation method that is applicable to OFDM, AFDM and OTFS in an iterative

turbo receiver architecture is proposed, that exchanges extrinsic information between the demapper and the channel decoder. Soft-MMSE refers to the holistic MMSE solution that updates its MMSE weighting matrix based on both the channel condition and the *a priori* probabilities gleaned from the channel decoder. EXIT chart analysis is performed to investigate the performance of Recursive Systematic Convolutional (RSC)-coded OFDM, AFDM and OTFS. Moreover, Unity Rate Convolutional (URC) coding is harnessed in order to improve the decoding convergence.

• It is demonstrated that for low-complexity transceivers having high coding rates, AFDM configurations exhibit a lower BER than their OTFS counterparts. Hence

AFDM is better suited to low-complexity systems than OTFS at significant velocities.

H. Notations

In the following sections, italics are used for scalar values (a/A), vectors are in lower case bold (a), matrices are in upper case bold (A), the transpose operation is denoted by $(\cdot)^T$, the complex conjugate operation is denoted by $(\cdot)^*$, the complex conjugate/Hermitian transpose is $(\cdot)^H$, and the matrix inverse is $(\cdot)^{-1}$. DD variables are denoted with a tilde (\tilde{a}) , AFD variables with two dots (\ddot{a}) , and TD variables are plain symbols (a).

II. Transmit Signal Model

The data bit vector $\boldsymbol{b}_D \in \mathbb{R}^{R_c B_S \ddot{N} \Xi \times 1}$ is encoded to produce the transmit bit vector $\boldsymbol{b} \in \mathbb{R}^{B_S \ddot{N} \Xi \times 1}$, where R_c is the channel coding rate, $B_S = log_2(\Gamma)$ is the number of bits per symbol, Γ is the modulation order, N is the number of AFDM chirp subcarriers, and Ξ is the number of transmission blocks within a frame. A transmission block refers to a set of N symbols (or equivalent for other waveforms) sent by the transmitter, and the channel parameters are assumed to be constant for the Ξ transmission blocks within a frame.

The transmit bits b are then interleaved using a random interleaver, where the interleave pattern is generated by a random number generator following a normal distribution, in order to generate b. When URC coding is employed in conjunction with another coding method, a second interleaving operation is performed after URC encoding using a second random interleaver. The block diagrams of RSC-AFDM and RSC-URC-AFDM are shown in Figures 1 and 2, respectively.

The interleaved bits $\stackrel{\infty}{b}$ are modulated using Phase Shift Keying (PSK) or Quadrature Amplitude Modulation (QAM) to form the AFD transmit signal $\ddot{x} \in \mathbb{C}^{\ddot{N}\Xi \times 1}$. \ddot{x} is then converted to the TD:

$$\boldsymbol{x}_{\xi} = \boldsymbol{A}_{\ddot{N}}^{H} \ddot{\boldsymbol{x}}_{\xi} , \qquad (1)$$

where $oldsymbol{x}_{\xi} \in \mathbb{C}^{\ddot{N} imes 1}$ is the TD transmit signal for the $\xi^{ ext{th}}$ transmit block, $\xi = [0, 1, ..., \Xi - 1]$ is the block index, and $A_{\ddot{N}}$ is the $N \times N$ DAFT, defined as:

$$\mathbf{A}_{\ddot{N}} = \mathbf{\Lambda}_{c_2} \mathbf{F}_{\ddot{N}} \mathbf{\Lambda}_{c_1} , \qquad (2)$$

where $m{F}_{\ddot{N}}$ is the $\ddot{N} \times \ddot{N}$ DFT, c_1 and c_2 are the chirp parameters 1 and 2, and:

$$\mathbf{\Lambda}_c = \operatorname{diag}(e^{-j2\pi c(\ddot{n})^2}) , \qquad (3)$$

where $\ddot{n} = [0, 1, ..., \ddot{N} - 1]$ is the AFDM chirp subcarrier index, and diag(v) generates a square diagonal matrix whose diagonal elements are the elements of v.

Following the conditions outlined in [13], c_1 is set to:

$$c_1 = \frac{2(\ddot{k}_{max} + k_{\nu}) + 1}{2\ddot{N}} , \qquad (4)$$

where \tilde{k}_{max} is the maximum AFDM Doppler index, defined in (18) further below, and k_{ν} is the AFDM guard for fractional indices.

Furthermore, c_2 is set to a small arbitrary irrational

$$c_2 = \frac{1}{9^{2\pi}} \ . \tag{5}$$

Detailed information on the basic concepts of the DAFT and of AFDM can be found in [13].

III. Channel and Received Signal Model

It is assumed that there is no external interference during transmission, that the CPP for AFDM and the CP for OTFS and OFDM are perfectly removed, and that their lengths are in excess of the maximum channel delay-spread.

The transmitted signal is passed through a typical timevarying and frequency-selective fading channel used in the OTFS literature, as modelled in [38]. The TD representation of this channel for OTFS is:

$$h_{m,n,p,\xi} = \widetilde{h}_p e^{j2\pi \widetilde{k}_p \frac{\xi MN + nM + m - \widetilde{l}_p}{MN}} , \qquad (6)$$

where $j = \sqrt{-1}$, p = [0, 1, ..., P-1] is the propagation path index, P is the total number of propagation paths, m = [0, 1]1, ..., M-1 denotes the OTFS subcarrier index, M is the number of OTFS subcarriers, n = [0, 1, ..., N-1] is the OTFS symbol slot index, N is the number of OTFS symbol slots, $\xi = [0, 1, ..., \Xi - 1]$ is the block index, \widetilde{h}_p is the fading gain and path loss, while \widetilde{l}_p and \widetilde{k}_p are the OTFS delay and Doppler indices associated with the p^{th} propagation path respectively, defined as:

$$\widetilde{l}_p = (\Delta f M) \, \tau_p \,\,, \tag{7}$$

$$\widetilde{l}_{p} = (\Delta f M) \tau_{p} , \qquad (7)$$

$$\widetilde{k}_{p} = \frac{N}{\Delta f} \nu_{p} , \qquad (8)$$

where Δf is the OTFS subcarrier spacing, τ_p is the delay associated with the p^{th} path, and ν_p is the Doppler shift associated with the p^{th} path.

This representation assumes integer delay indices, as the delay resolution is assumed to be sufficiently large. The propagation path variables are assumed to be constant over the Ξ transmission blocks. The equivalent AFDM channel is attained upon substituting MN with N and Δf with Δf . Hence, the TD representation of the channel for AFDM is:

$$h_{\ddot{n},\,p,\,\xi} = \tilde{h}_p e^{j2\pi\vec{k_p} \frac{\xi \ddot{N} + \ddot{n} - \ddot{l_p}}{\ddot{N}}} , \qquad (9)$$

where $\ddot{l_p}$ and $\ddot{k_p}$ are the AFDM delay and Doppler indices associated with the p^{th} propagation path respectively:

$$\ddot{l_p} = \left(\ddot{\Delta f} \ddot{N}\right) \tau_p , \qquad (10)$$

$$\ddot{k_p} = \frac{\dot{\nu_p}}{\ddot{\Delta}f} \,, \tag{11}$$

where Δf is the AFDM subcarrier spacing.

Therefore, in order to have consistent delay and Doppler indices between (7)-(8) and (10)-(11), $\ddot{N} = MN$, $\ddot{n} = nM + m$ m, and $\Delta f = \frac{\Delta f}{N}$.

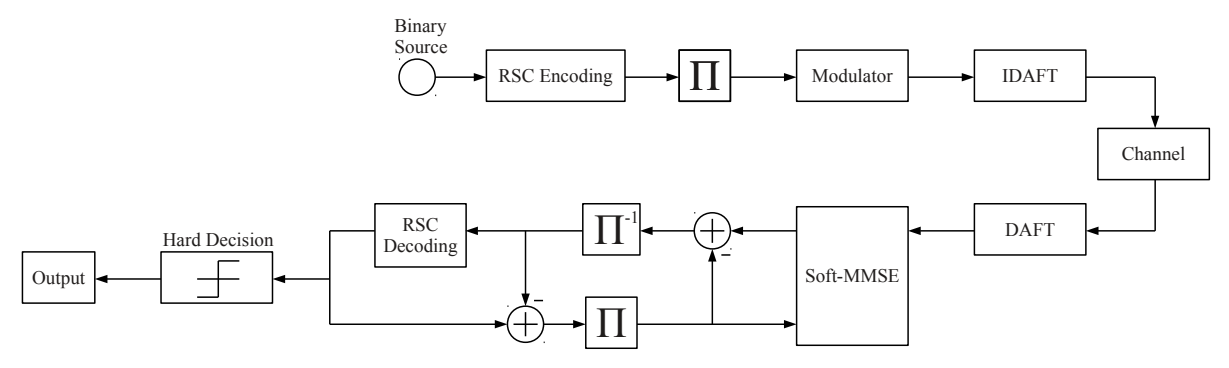


FIGURE 1: Block diagram of RSC-AFDM

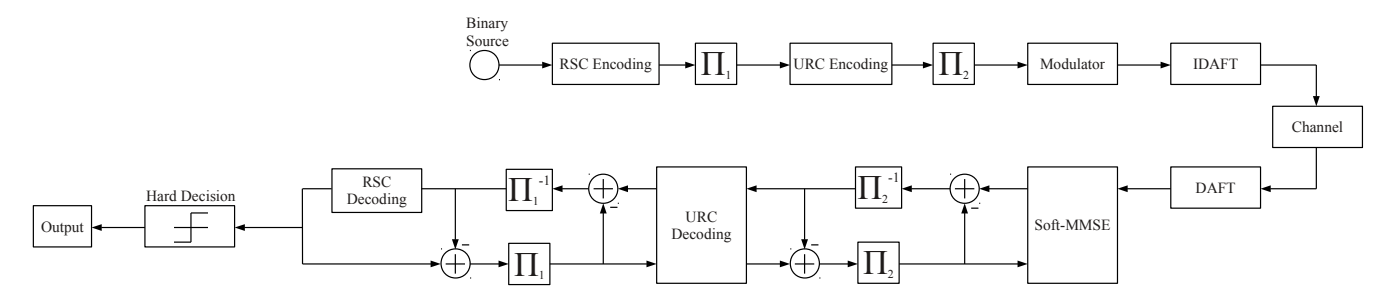


FIGURE 2: Block diagram of RSC-URC-AFDM

Each index can be decomposed into its integer- and fractionally-spaced counterparts, e.g.:

$$\widetilde{k}_p = \widetilde{k}_p + \delta \widetilde{k}_p , \qquad (12)$$

where the $\widetilde{\underline{k}_p}=\lfloor\widetilde{k}_p
ceil$ is the integer part of the index, $\delta\widetilde{k}_p=\widetilde{k}_p-\widetilde{k}_p$ is the fractional component, and $\lfloor\cdot\rceil$ is the rounding function.

Using this notation, the TD channel representations in (6) and (9) can be respectively rewritten as:

$$h_{m,n,p,\xi} = \left(\widetilde{h}_p e^{j2\pi \widetilde{k}_p \frac{nM+m-\widetilde{l}_p}{MN}}\right) e^{j2\pi \delta \widetilde{k}_p \xi} , \qquad (13)$$

$$h_{\ddot{n},p,\xi} = \left(\widetilde{h}_p e^{j2\pi \vec{k}_p \frac{\vec{n} - l_p^r}{\vec{N}}}\right) e^{j2\pi \delta \vec{k}_p \xi} . \tag{14}$$

It can be readily seen that when the fractional component of the Doppler indices is 0, the channel does not vary with respect to the block index ξ . When δk_p is non zero, the additional blocks impose a phase shift to the TD channel.

The channel is specifically defined for OTFS and AFDM for explicit clarity, since multiple OTFS and AFDM configurations are considered, as shown in Table 2. When $\ddot{N}=MN$, $\ddot{n}=nM+m$, and $\ddot{\Delta f}=\frac{\Delta f}{N}$, the TD channels in (13) and (14) of AFDM and OTFS are equal to each other. The equivalence described in this paper between the two waveforms is based on the channel, and therefore on the input-output relationship of the waveforms. The OTFS TD channel representation is also directly applied to OFDM, as OTFS and OFDM utilise the same system parameters.

A. Propagation Path Parameter Generation

The first path p=0 is the Line of Sight (LoS) path, while the remaining P-1 paths are NLoS paths. The fading gain and path loss \widetilde{h}_{p} is:

$$\widetilde{h}_{p} = \begin{cases}
\sqrt{\frac{\kappa}{\kappa+1}}, & \text{if } p = 0 \\
\sqrt{\frac{1}{(\kappa+1)(P-1)}}\zeta_{p}, & \text{if } p > 0
\end{cases},$$
(15)

where κ is the Rician K factor, and ζ_p is a complex Gaussian random variable with mean $\mu_h = 0$ and variance $\sigma_h^2 = 1$, expressed as $\mathcal{CN}(\mu_h, \sigma_h^2)$.

The LoS path has a gain of 1 as the signal propagates directly from the transmitter to the receiver. Hence, it is assumed that only the delay and Doppler shift distort the signal. In the NLoS paths, the signal propagates through a random set of paths, each with their own phase shifts and path losses. As these paths are not known, the random phase shift and path loss are generated using a Gaussian variable, with the overall average power dictated by the Rician K factor.

The delay index l_n is:

$$l_p = \begin{cases} 0, & \text{if } p = 0\\ \lfloor (D_T - 1)\eta_l \rceil, & \text{if } p > 0, \end{cases}$$
 (16)

where D_T is the number of delay taps, and η_l is a random variable obeying a uniform distribution between 0 and 1.

The number of delay taps D_T defines the maximum delay index, and hence the maximum propagation path delay. No pair of propagation paths will have the same delay index,

yielding: $l_{p_1} \neq l_{p_2}$, where $p_1 = [0, 1, \dots P-1]$, $p_2 = [0, 1, \mathcal{L}_{\xi}^{\alpha, \mu}]$ for the ξ^{th} transmit block as: ... P-1], and $p_1 \neq p_2$.

The fractional Doppler index k_p is:

$$k_p = |2k_{max}(\eta_k - 0.5)|,$$
 (17)

where η_k is a random variable following a uniform distribution between 0 and 1, and k_{max} is the maximum integer Doppler index, defined as:

$$k_{max} = \lfloor \frac{1}{\ddot{\Delta}f} \frac{f_c V}{c_0} \rceil = \lfloor \frac{N}{\Delta f} \frac{f_c V}{c_0} \rceil , \qquad (18)$$

where V is the velocity of the communication receiver, f_c is the carrier frequency, and c_0 is the speed of light. The equality holds when equivalent AFDM and OTFS configurations are compared.

B. Channel Matrix and Received Signal Definition

The TD channel matrix for the p^{th} path and block ξ , $\boldsymbol{H}_{p,\xi} \in$ $\mathbb{C}^{\ddot{N}\times\ddot{N}}$, is formulated as:

$$\boldsymbol{H}_{p,\,\xi}[\ddot{n},\,\lfloor \ddot{n} - \ddot{l}_{p}^{\prime} \rfloor_{\ddot{N}}] = h_{\ddot{n},\,p,\,\xi} \,\,, \tag{19}$$

where $|\cdot|_{\ddot{N}}$ is the modulo \ddot{N} operator.

The TD channel matrix for all paths for the block ξ , H_{ξ} \in $\mathbb{C}^{\ddot{N} \times \ddot{N}}$, is the superposition of the individual path channel matrices, formulated as:

$$H_{\xi} = \sum_{p=0}^{P-1} H_{p,\xi} .$$
 (20)

For OTFS, the $h_{\ddot{n},\,p,\,\xi}$ is replaced by $h_{m,\,n,\,p,\,\xi}$, with nM+m instead of \ddot{n} , \ddot{N} substituted by MN, and the OTFS delay and Doppler indices utilised.

The TD received signal for block ξ , $y_{\xi} \in \mathbb{C}^{\ddot{N} \times 1}$, is:

$$\boldsymbol{y}_{\varepsilon} = \boldsymbol{H}_{\varepsilon} \boldsymbol{x}_{\varepsilon} + \boldsymbol{z}_{\varepsilon} , \qquad (21)$$

where z_{ξ} is the complex-valued Additive White Gaussian Noise (AWGN) for block ξ , with mean $\mu_z = 0$ and variance N_0 , expressed as $\mathcal{CN}(\mu_z, N_0)$, and N_0 is the noise power.

The AFD received signal for block ξ , $\ddot{\boldsymbol{y}}_{\xi} \in \mathbb{C}^{N \times 1}$, is:

$$\ddot{\boldsymbol{y}}_{\xi} = \boldsymbol{A}_{\ddot{N}} \boldsymbol{y}_{\xi} = \boldsymbol{A}_{\ddot{N}} \boldsymbol{H}_{\xi} \boldsymbol{A}_{\ddot{N}}^{H} \ddot{\boldsymbol{x}}_{\xi} + \boldsymbol{A}_{\ddot{N}} \boldsymbol{z}_{\xi},$$

$$\ddot{\boldsymbol{y}}_{\varepsilon} = \ddot{\boldsymbol{H}}_{\varepsilon} \ddot{\boldsymbol{x}}_{\varepsilon} + \boldsymbol{A}_{\ddot{N}} \boldsymbol{z}_{\varepsilon},$$
(22)

where $\ddot{\boldsymbol{H}}_{\xi}$ is the AFD equivalent channel:

$$\ddot{\boldsymbol{H}}_{\xi} = \boldsymbol{A}_{\ddot{N}} \boldsymbol{H}_{\xi} \boldsymbol{A}_{\ddot{N}}^{H} . \tag{23}$$

IV. Soft-MMSE Detection

Soft-MMSE equalisation [39] is applied at the receiver, with perfect channel estimation assumed. Due to the interleaving applied to the coded bits, the channel decoder's a posteriori Log-Likelihood Ratios (LLRs) $\mathcal{L}^{\rho,\delta}$ are interleaved to generate the soft-MMSE a priori LLRs $\mathcal{L}^{\alpha,\mu}$.

For each transmit block ξ , a transmit symbol estimate $\varepsilon\{\ddot{x}_{\varepsilon}\}$ is formulated using the soft-MMSE a priori LLRs

$$\varepsilon\{\ddot{\boldsymbol{x}}_{\xi}[\ddot{n}]\} = \sum_{\gamma=0}^{\Gamma-1} s_{\gamma} \mathcal{P}\left(\ddot{\boldsymbol{x}}_{\xi}[\ddot{n}] = s_{\gamma}\right) ,$$

$$= \sum_{\gamma=0}^{\Gamma-1} s_{\gamma} \frac{\exp\left(\sum_{\beta=0}^{B_{S}-1} b_{\beta}^{\gamma} \mathcal{L}_{\xi}^{\alpha,\mu}[\ddot{n}B_{S} + \beta]\right)}{\prod_{\beta=0}^{B_{S}-1} \left(1 + \exp\left(\mathcal{L}_{\xi}^{\alpha,\mu}[\ddot{n}B_{S} + \beta]\right)\right)} ,$$
(24)

where $\mathcal{P}\left(a=b\right)$ denotes the probability of $a=b,\ s_{\gamma}$ is the modulated symbol corresponding to the integer value γ , $\gamma = [0, 1, ..., \Gamma - 1]$ is the modulation index, $\beta = [0, 1, ...]$ B_S-1 is the index of bits in a symbol, and $\exp(\cdot)$ is the natural exponential function.

A diagonal matrix E of the squared magnitude of $\varepsilon\{\ddot{x}_{\varepsilon}\}$ is then generated as:

$$\boldsymbol{E} = \operatorname{diag}\left(\varepsilon\{\ddot{\boldsymbol{x}}_{\varepsilon}\} \otimes \varepsilon\{\ddot{\boldsymbol{x}}_{\varepsilon}\}^{*}\right) , \qquad (25)$$

where \otimes is the element-wise multiplication, and $(\cdot)^*$ is the complex conjugate operation.

The AFDM MMSE matrix \hat{G}_{ξ} for the ξ^{th} transmit block

$$\ddot{\boldsymbol{G}}_{\xi} = \left(\ddot{\boldsymbol{H}}_{\xi}^{*} \left(\boldsymbol{R}_{SX} + \boldsymbol{E}\right) \ddot{\boldsymbol{H}}_{\xi}^{T} + N_{0} \boldsymbol{I}_{\ddot{N} \times \ddot{N}}\right)^{-1} \ddot{\boldsymbol{H}}_{\xi}^{*}, \quad (26)$$

where $(\cdot)^T$ is the transpose operation, ${\pmb I}_{\ddot{N}\times \ddot{N}}$ is the $\ddot{N}\times \ddot{N}$ identity matrix, and $oldsymbol{R}_{SX}$ is the covariance matrix of the transmit symbols, which is set to $I_{\ddot{N}\times \ddot{N}}$, since the average transmit symbols power is normalised to 1.

The soft-MMSE transmit signal estimate \hat{x} is expressed:

$$\overset{\mu}{\boldsymbol{x}}[\ddot{n}] = \left(\left(\ddot{\boldsymbol{y}}_{\xi} \right)^{T} \ddot{\boldsymbol{g}}_{\xi,\ddot{n}} - \iota_{\xi,\ddot{n}} \right) \frac{\begin{pmatrix} \mu \\ h_{\xi,\ddot{n}} \end{pmatrix}^{*}}{|h_{\xi,\ddot{n}}|^{2}} , \qquad (27)$$

where $|\cdot|$ is the magnitude operator, $\ddot{g}_{\xi,\ddot{n}}$ is the \ddot{n}^{th} column of \ddot{G}_{ξ} , $\iota_{\xi,\ddot{n}}$ is the interference imposed upon the \ddot{n}^{th} symbol by the other $\ddot{N}-1$ symbols in the ξ^{th} transmit block, and $h_{\xi,\ddot{n}}$ is:

$$\overset{\mu}{h}_{\xi,\ddot{n}} = \left(\ddot{\boldsymbol{h}}_{\xi,\ddot{n}} \right)^T \ddot{\boldsymbol{g}}_{\xi,\ddot{n}} . \tag{28}$$

The interference imposed upon the \ddot{n}^{th} symbol by the other $\ddot{N}-1$ symbols in the ξ^{th} transmit block $\iota_{\xi,\ddot{n}}$ is:

$$\iota_{\xi,\ddot{n}} = \sum_{\ddot{n}_2 = 0, \ddot{n}_2 \neq \ddot{n}}^{\ddot{N} - 1} \varepsilon \{ \ddot{\boldsymbol{x}}_{\xi} [\ddot{n}_2] \} \left(\ddot{\boldsymbol{h}}_{\xi, \ddot{n}_2} \right)^T \ddot{\boldsymbol{g}}_{\xi, \ddot{n}} . \tag{29}$$

The equivalent soft-MMSE AWGN noise power $N_{0,\xi}$ for each symbol is expressed as:

$$\overset{\mu}{N}_{0,\xi}[\ddot{n}] = \frac{1}{|h_{\xi,\ddot{n}}|} + (E[\ddot{n},\ddot{n}] - 1) . \tag{30}$$

The approximate maximum probability metric $d_{\frac{\mu}{m}}$ describing the probability of the transmit symbol $\ddot{x}[m]$ being

TABLE 3: Lookup table for the Jacobian algorithm

Value of $ d_1 - d_2 $	Value of $\Theta(d_1 - d_2)$				
$ d_1 - d_2 > 3.7$	0				
$2.25 < d_1 - d_2 \le 3.7$	0.05				
$1.5 < d_1 - d_2 \le 2.25$	0.15				
$1.05 < d_1 - d_2 \le 1.5$	0.25				
$0.7 < d_1 - d_2 \le 1.05$	0.35				
$0.43 < d_1 - d_2 \le 0.7$	0.45				
$0.2 < d_1 - d_2 \le 0.43$	0.55				
$ d_1 - d_2 \le 0.2$	0.65				

 s_{γ} can then be generated using $\overset{\mu}{x}[\overset{\mu}{m}]$ and $\overset{\mu}{N}_{0,\xi}$:

$$d_{m,\gamma}^{\mu} = -\frac{\left|\mathbf{x}[m] - s_{\gamma}\right|^{2}}{\mathbf{N}_{0}[m]} + \sum_{\beta=0}^{B_{S}-1} b_{\beta}^{\gamma} \mathcal{L}_{\xi}^{\alpha,\mu}[\ddot{b}] , \quad (31)$$

where $\ddot{b}=[0,\ 1,\ ...,\ \ddot{N}B_S-1]$ is the bit index within the transmit block $\xi,\ m=\lfloor\frac{\ddot{b}}{B_S}\rfloor$, and $\lfloor\cdot\rfloor$ is the floor function.

The soft-MMSE *a posteriori* LLRs $\mathcal{L}_{\xi}^{\rho,\mu}$ for the ξ^{th} transmit block are then calculated using the Approx-Log-MAP algorithm from [39], [40]:

$$\mathcal{L}_{\xi}^{\rho,\mu}[\ddot{b}] = \operatorname{jac}\begin{pmatrix} \mu \\ d_{m,\gamma} \\ s_{\gamma} \in \mathcal{S}_{b_{\xi}=1} \end{pmatrix} - \operatorname{jac}\begin{pmatrix} \mu \\ d_{m,\gamma} \\ s_{\gamma} \in \mathcal{S}_{b_{\xi}=0} \end{pmatrix}, \qquad (32)$$

where $jac(\cdot)$ is the Jacobian function:

$$jac (d_1, d_2) = \max (d_1, d_2) + \Theta (|d_1 - d_2|) , \qquad (33)$$

where max is the maximum function that returns the highest value, and $\Theta(|d_1 - d_2|)$ is an additional term whose value is specified by Table 3 [41], [42].

The soft-MMSE algorithm outputs the *a posteriori* LLRs for the Ξ transmit blocks $\mathcal{L}^{\rho,\mu} \in \mathbb{R}^{R_c B_s \ddot{N}\Xi \times 1}$. The *a posteriori* LLRs $\mathcal{L}^{\rho,\mu}$ are then de-interleaved to produce the channel decoder's *a priori* LLRs $\mathcal{L}^{\alpha,\delta}$, which are then passed to the RSC decoder when RSC coding is employed, or to the URC decoder when RSC-URC coding is utilised, as shown in Figures 1 and 2, respectively. For AFDM, the *a posteriori* LLRs are $\ddot{\mathcal{L}}^{\rho,\mu} \in \mathbb{R}^{R_c B_s \ddot{N}\Xi \times 1}$, whereas for OTFS, they are $\tilde{\mathcal{L}}^{\rho,\mu} \in \mathbb{R}^{R_c B_s MN\Xi \times 1}$. The soft-MMSE method presented is used for AFDM, OTFS, and OFDM, as it is independent of the waveform or signal domain.

V. Simulation Results

The simulation parameters are shown in Table 4. The number of subcarriers refers to OFDM-type subcarriers for OFDM and OTFS, and to chirp subcarriers for AFDM. Different random interleavers are generated for each frame. The same interleaver is utilised across transmission blocks within a frame, and the interleaver length is 10 000 bits.

The five configurations outlined in Table 2 are characterised by simulations. OFDM is configured to match OTFS 1, with multiple symbol slots. AFDM 1 is equivalent

to OTFS 1, hence it possesses a smaller subcarrier spacing than OFDM and OTFS 1, to ensure that the same frequency resources are utilised. The duration of AFDM 2 is equal to that of a single OFDM symbol, and has the same subcarrier spacing as OFDM. OTFS 2 is the configuration that is equivalent to AFDM 2. OTFS 3 has the same matrix dimension and subcarrier spacing as AFDM 1, hence it has a lower bandwidth. OTFS 3 is included since some references utilise this OTFS configuration to compare with AFDM.

Four parameter value groups are investigated, named Set 1, 2, 3, and 4. The matrix dimensions of OFDM, OTFS 1, and AFDM 1 are divided by 4 every time the Set index is increased. The values of the base variables defined in Table 2 are, for each Set:

- Set 1: M = 32, N = 16, $\Delta f = 15$ kHz.
- Set 2: M = 16, N = 8, $\Delta f = 30$ kHz.
- Set 3: M = 8, N = 4, $\Delta f = 60$ kHz.
- Set 4: M = 4, N = 2, $\Delta f = 120$ kHz.

A. Uncoded BER

The BERs of uncoded Binary Phase Shift Keying (BPSK) AFDM 1 and 2, OTFS 1, 2, and 3, and OFDM utilising hard-MMSE are shown in Figure 3. The BER of OFDM using single tap Frequency Domain (FD) equalisation, denoted as "FDE", is also shown. Hard-MMSE refers to the MMSE equalisation that outputs bit estimates (hard values), as opposed to LLRs (soft values). For Set 1, the BERs of the AFDM and OTFS configurations are similar to each other. The BER of hard-MMSE OFDM is higher than that of AFDM and OTFS, with the BER of "FDE" OFDM remaining above 0.3 for the Energy per bit over Noise power (E_b/N_0) range considered.

When the Set index is increased, the dimension of the configurations is reduced, and the BERs of the AFDM configurations do not increase to the same extent as the BERs of their OTFS counterparts at high E_b/N_0 . AFDM 1 is the counterpart to OTFS 1, and AFDM 2 is the counterpart to OTFS 2. OTFS 3 has no direct counterpart, and it is included to illustrate how a non-equivalent configuration may result in an unfair comparison between OTFS and AFDM. OTFS 3 has the same subcarrier spacing and dimension as AFDM 1, which results in OTFS 3 possessing a smaller bandwidth than AFDM 1.

It can be observed from Figure 3 that for Set 1, associated with the largest matrix dimension, AFDM 1 and OTFS 1 exhibit a similar BER, while the BER of AFDM 2 is comparable to that of OTFS 2. However, as the matrix dimension is reduced from that of Set 1 to Set 4, the AFDM configurations gradually start to outperform their OTFS counterparts. This is because to AFDM's diversity gain only presenting a significant advantage when the codeword differences are small, for small matrix dimensions. Therefore, Set 4 is utilised for the majority of the following results, as it is the parameter Set for which AFDM exhibits the most substantial BER improvement over OTFS.

TABLE 4: Simulation parameter values								
Parameter	OFDM	AFDM 1	OTFS 1	AFDM 2	OTFS 2	OTFS 3		
Modulation order Γ	2							
Number of propagation paths P	4							
Number of delay taps D_T			5	5				
Communication receiver velocity V			150	m/s				
Rician K factor κ			0 0	iВ				
Carrier frequency f_c	38.5 GHz							
Maximum propagation delay $ au_{max}$	$10.4167~\mu s$							
AFDM guard for fractional indices $k_{ u}$	N/A	1	N/A	1	N/A	N/A		
		Set 1						
Number of subcarriers	32	512	32	32	8	32		
Number of symbol slots	16	N/A	16	N/A	4	16		
Subcarrier spacing	15 kHz	$\frac{15}{16}$ kHz	15 kHz	15 kHz	60 kHz	$\frac{15}{16}$ kHz		
		Set 2						
Number of subcarriers	16	128	16	16	8	16		
Number of symbol slots	8	N/A	8	N/A	2	8		
Subcarrier spacing	30 kHz	$\frac{15}{4}$ kHz	30 kHz	30 kHz	60 kHz	$\frac{15}{4}$ kHz		
Set 3								
Number of subcarriers	8	32	8	8	4	8		
Number of symbol slots	4	N/A	4	N/A	2	4		
Subcarrier spacing	60 kHz	15 kHz	60 kHz	60 kHz	120 kHz	15 kHz		
Set 4								
Number of subcarriers	4	8	4	4	2	4		
Number of symbol slots	2	N/A	2	N/A	2	2		
Subcarrier spacing	120 kHz	60 kHz	120 kHz	120 kHz	240 kHz	60 kHz		

TABLE 4: Simulation parameter values

B. EXIT Chart Analysis

The EXIT charts of Set 4 soft-MMSE BPSK AFDM 1 and 2, OTFS 1, 2, and 3, and OFDM for 0 dB E_b/N₀ are shown in Figure 4. As expected, the *a posteriori* mutual information is increased when the *a priori* mutual information is increased. This demonstrates that the soft-MMSE method is capable of improving the performance compared to hard MMSE. The EXIT curves of AFDM 1 and OTFS 1 are similar to each other, indicating a similar performance. The EXIT curve of AFDM 2 has a steeper gradient than that of OTFS 2, which suggests that AFDM 2 has a superior detection capability to OTFS 2. The EXIT curve of soft-MMSE OFDM is at a higher ordinate value than that of hard-MMSE OFDM, but maintains the same 0 gradient, which indicates that soft-MMSE OFDM cannot provide an iteration gain. The EXIT curve of soft-MMSE OFDM is also at a lower ordinate value than those of AFDM and OTFS. The lack of gradient in the soft-MMSE OFDM EXIT curve is due to the lack of correlation between the OFDM subcarriers, when no AFDM or OTFS precoding is implemented.

The EXIT charts and trajectories of Set 4 RSC- and RSC-URC-coded BPSK AFDM 1, OTFS 1 and OFDM for soft-MMSE are shown in Figure 5, for 4 dB E_b/N_0 . The trajectories of AFDM 1 and OTFS 1 are similar, which reflects the general trend of approximately similar performance between

AFDM and OTFS. Due to the flat EXIT chart of soft-MMSE OFDM, there is little iterative gain is attained for RSC coding.

The trajectories of RSC coding reach their end points in 1 or 2 iterations for AFDM 1 and OTFS 1. At a coding rate of 0.9, the minimum *a posteriori* mutual information is 0.9, which only leaves room for modest iteration gain. Hence, the RSC coded AFDM 1 and OTFS 1 trajectories approach the ideal (1, 1) point of perfect convergence.

When URC is harnessed, the EXIT chart performance of soft-MMSE is improved for all three waveforms for $R_c=0.5$, which leads to a higher iterative gain for RSC coding, as the trajectory end point is closer to the ideal (1, 1) point. This is a benefit of the URC increasing the open tunnel. A greater number of iterations is required to reach the (1, 1) point when URC is employed, but this phenomenon no longer persists at higher coding rates, as shown in Figure 5b for $R_c=0.9$, as the initial *a posteriori* mutual information is very high (0.9). The performance of RSC-URC-OFDM remains lower than that of RSC-URC-AFDM 1 and RSC-URC-OTFS 1.

C. Comparison of RSC and RSC-URC AFDM

The BERs of Set 4 RSC- and RSC-URC-coded BPSK AFDM 1 and 2 are shown in Figure 6, for $R_c=0.5$ and 0.9. "RSC-AFDM 1 it" refers to RSC-AFDM relying on

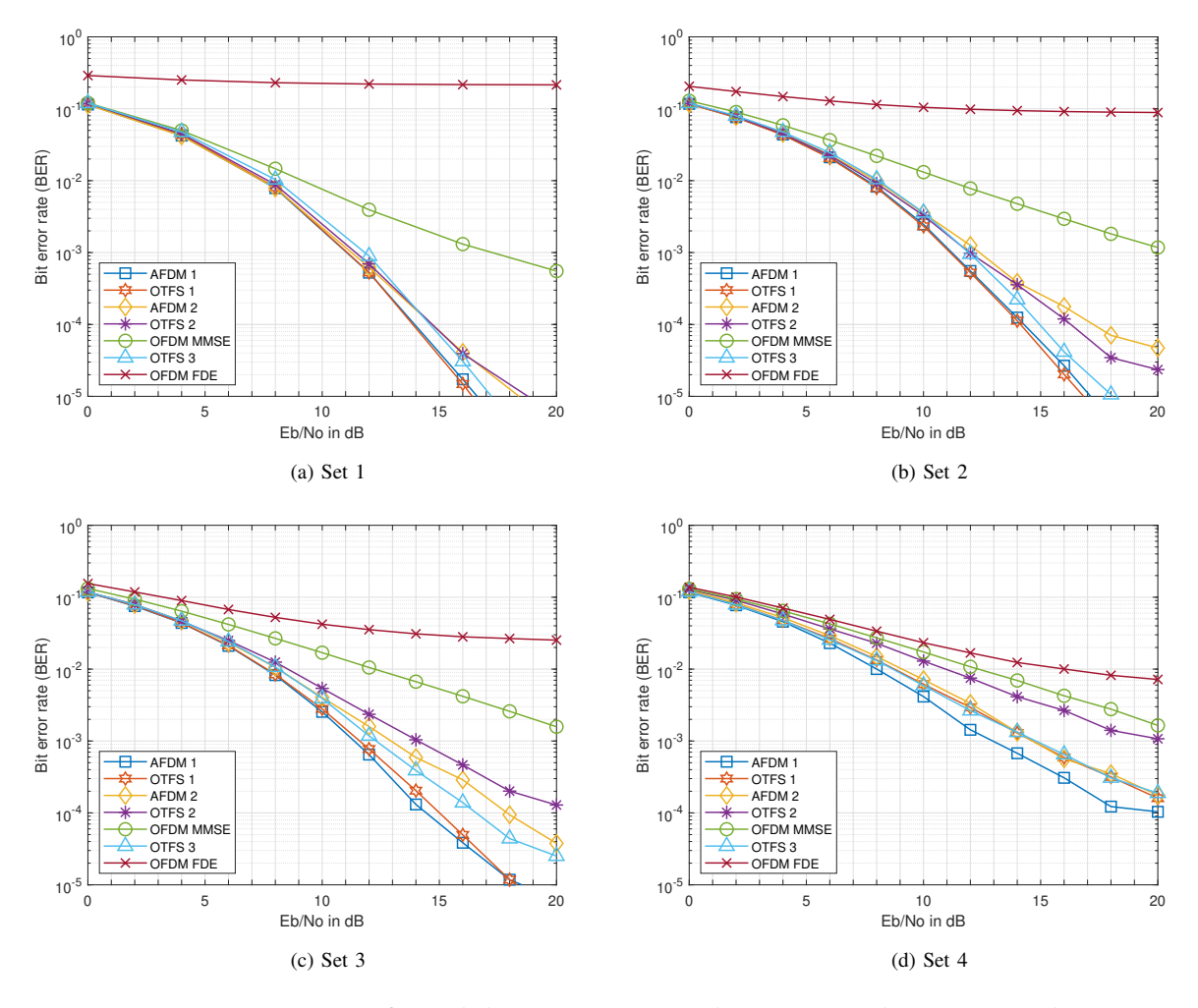


FIGURE 3: BER of uncoded BPSK AFDM 1 and 2, OFDM, and OTFS 1, 2 and 3

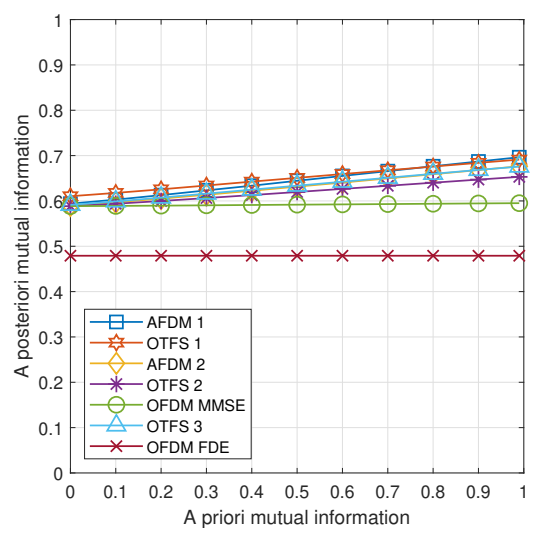


FIGURE 4: EXIT chart of Set 4 soft-MMSE BPSK AFDM 1 and 2, OFDM, and OTFS 1 and 2 for 0 dB E_b/N_0

a single iteration, and "RSC-URC-AFDM 2/4 it" refers to RSC-URC-AFDM having 2 inner and 4 outer iterations. For RSC-URC coding, the inner iterations are between URC decoding and soft-MMSE equalisation. The outer iterations are between the RSC decoder and the combined URC-equaliser block.

As expected, increasing the coding rate increases the BER for both AFDM configurations and for both coding methods. The BER of RSC-AFDM 1 is lower than that of RSC-AFDM 2 at high $\rm E_b/N_0$ and for a sufficiently high number of iterations, following the trend for uncoded hard-MMSE AFDM simulated with the Set 4 variable values. The BER difference is accentuated when the coding rate is increased, as fewer errors can be corrected at high coding rates. The BER of RSC-URC-AFDM 1 is lower than that of AFDM 2 for both coding rates and for the specific number of inner and outer iterations considered.

For RSC coding, increasing the number of iterations from 1 to 2 drastically reduces the BER for both coding rates. By contrast, increasing the number of iterations from 2 to 4 no

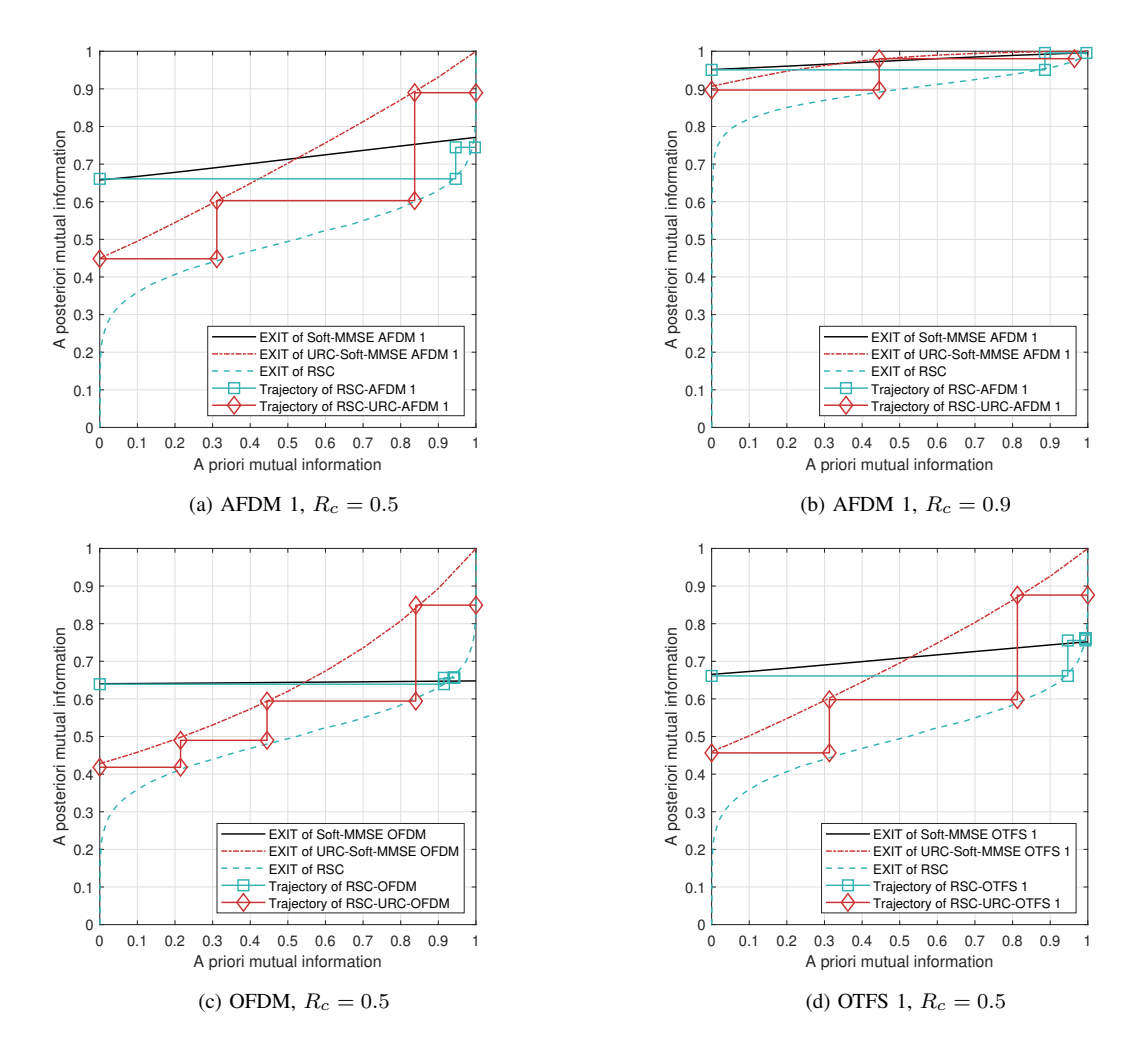


FIGURE 5: EXIT chart and trajectory of Set 4 RSC- (square) and RSC-URC-coded (diamond) BPSK AFDM 1, OFDM, and OTFS 1 for 4 dB E_b/N_0

longer significantly improves the BER for a coding rate of 0.5, but slightly lowers it for a coding rate of 0.9. This result is consistent with the EXIT chart based prediction, where the trajectory end point is reached within a low number of iterations. The drastic BER reduction of RSC coding as the number of iterations increases is indeed expected as an explicit benefit of having iteratively improved extrinsic LLRs.

The BER of RSC-URC coding is higher for both coding rates than that of stand-alone RSC coding when a similar complexity is considered, which is a plausible reflection of the fact that RSC-URC can only improve the BER at an increased complexity. To elaborate, at a coding rate of 0.5, the BER of RSC-URC coding decreases as the number of outer iterations is increased up to 8. Further increase in the number of iterations does not significantly improve the BER performance. Again, RSC-URC is capable of outperforming RSC coding at the lower coding rates, but only at higher numbers of iterations. This is consistent with the EXIT chart

predictions, where the trajectory end point for RSC-URC is only reached at a higher number of iterations than for RSC coding, but it is closer to the ideal $(1,\,1)$ point. At a coding rate of 0.9, the BER of RSC-URC is higher than that of RSC coding, even when a higher number of outer iterations is utilised. This is also shown in the EXIT chart results, where the addition of URC does not significantly impact the EXIT curve gradient of soft-MMSE equalisation at this coding rate. At small matrix dimensions, high code rates and many outer iterations, the BER of RSC-URC coding becomes unstable at high E_b/N_0 , as shown in Figure 6d.

D. BER of RSC-URC coded OFDM, AFDM, and OTFS

The BERs of Set 4 RSC-URC-coded BPSK AFDM 1 and 2, OFDM, and OTFS 1, 2, and 3 are shown in Figure 7, for coding rates of 0.5, 0.7, and 0.9, and for $It_{inner} = 2$, and $It_{outer} = 2$ and 8. For all coding rates and number of outer iterations, OFDM has the highest BER trend.

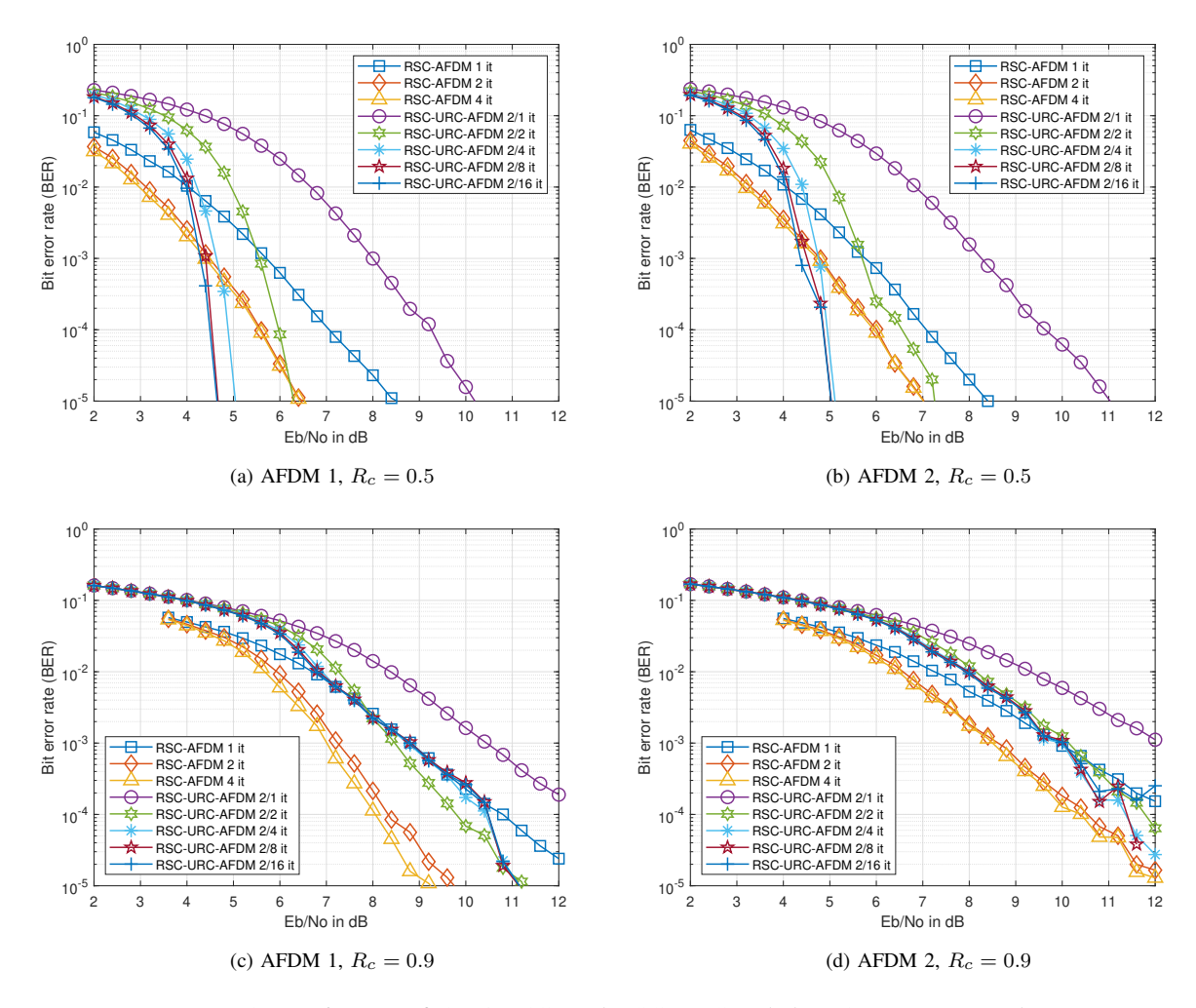


FIGURE 6: BER of Set 4 RSC- and RSC-URC-coded BPSK AFDM 1 and 2

TABLE 5: E_b/N_0 in dB at which a BER of 10^{-4} is achieved for RSC-URC coding, $R_c = 0.9$, 2 inner iterations, and 8 outer iterations

Set index	AFDM 1	OTFS 1	AFDM 2	OTFS 2	OTFS 3	OFDM MMSE
Set 1	6.6	6.9	6.7	6.85	6.8	10.2
Set 2	6.7	6.8	7	7	7.2	10.8
Set 3	6.8	6.9	10.2	10	7	11.4
Set 4	10.2	10	11.4	N/A	10	N/A

For $R_c=0.5$, the BER of AFDM 1, OTFS 1 and OTFS 3 are similar to each other, with OTFS 2, AFDM 2, and OFDM exhibiting a higher BER. For It_{outer} = 2, increasing R_c increases the relative BER difference of the configurations. AFDM 1 has the lowest BER, followed by OTFS 1 and 3, then AFDM 2, OTFS 2, and OFDM. Recall that AFDM 1, OTFS 1, and OTFS 3 have the larger matrix dimensions, hence they combat the effect of the channel and AWGN better, albeit at the expense of increased complexity. Furthermore, AFDM 2 and OTFS 2 have lower matrix dimensions, which leads to a higher BER, but a lower

complexity. At the high velocity considered, the subcarrier orthogonality of OFDM is partially compromised, leading to higher BERs. These trends follow those observed for uncoded transmissions in Figure 3d.

When the number of outer iterations is increased to $\rm It_{outer}$ = 8, the relative difference in BER between the configurations is reduced. The BER trends of AFDM 1, OTFS 1, and OTFS 3 are similar to each other. Observe that AFDM 2, OTFS 2, and OFDM have similar BER trends to each other for $R_c = 0.5$ and 0.7, with a higher BER than AFDM 1, OTFS 1, and OTFS 3. At $R_c = 0.9$, the BER of AFDM 2

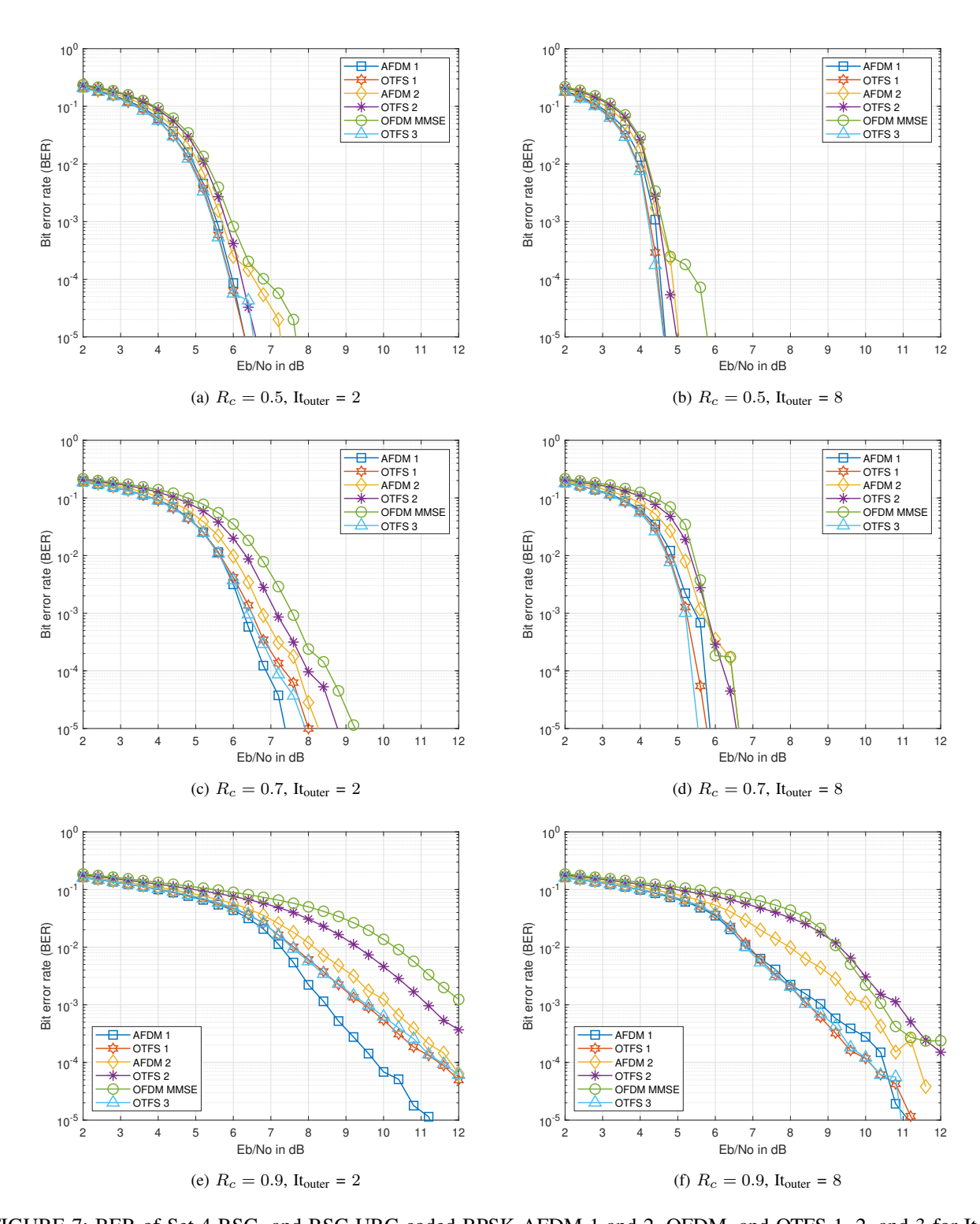


FIGURE 7: BER of Set 4 RSC- and RSC-URC-coded BPSK AFDM 1 and 2, OFDM, and OTFS 1, 2, and 3 for It_{inner} = 2

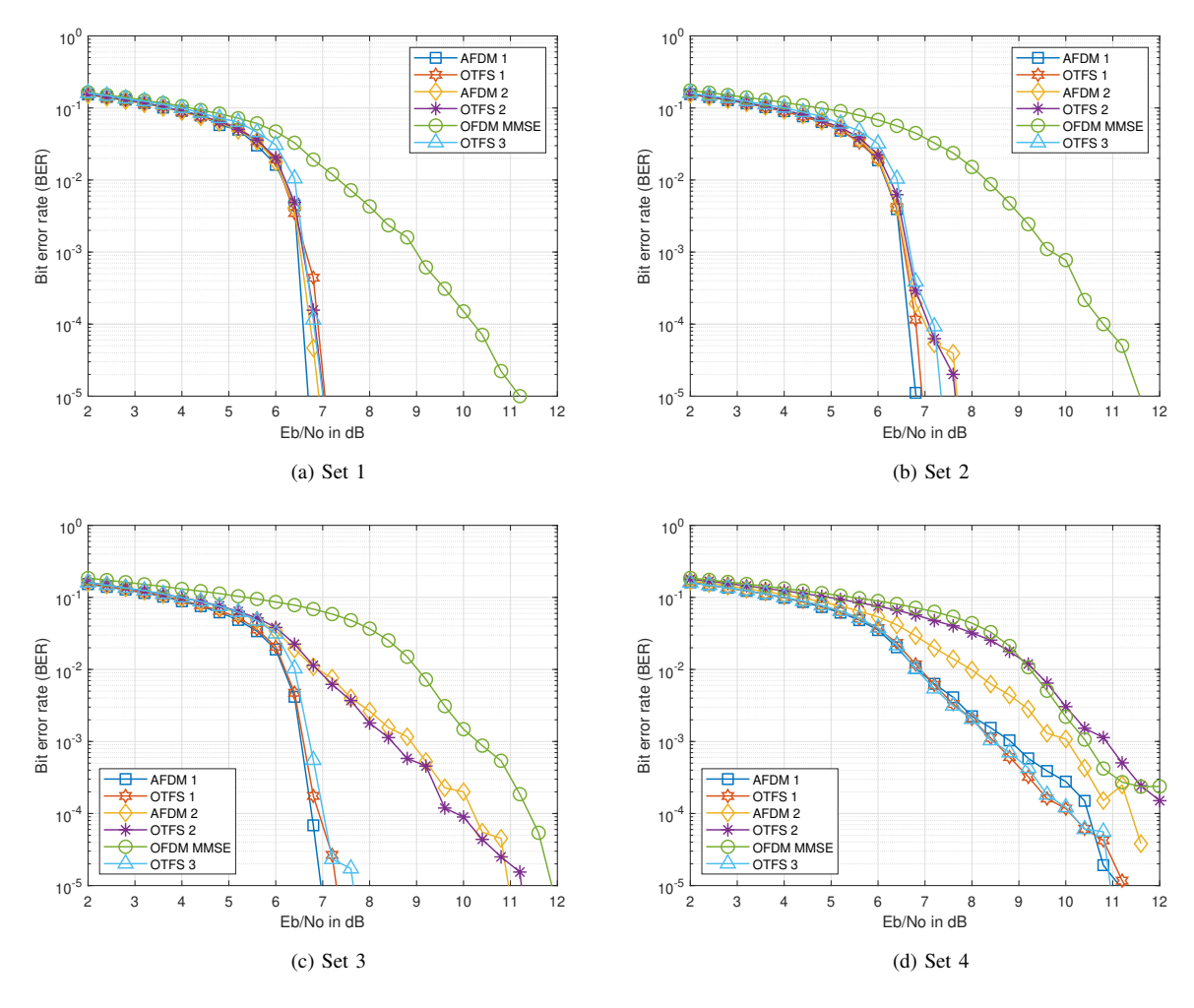


FIGURE 8: BER of Set 1, 2, 3, and 4 RSC-URC-coded BPSK AFDM 1 and 2, OFDM, and OTFS 1, 2 and 3 for $R_c = 0.9$ and $It_{inner} = 2$ and $It_{outer} = 8$ iterations

is higher than that of AFDM 1, OTFS 1, and OTFS 3, but lower than that of OTFS 2 and OFDM. This is an explicit benefit of AFDM's higher degrees of freedom than those of OTFS and OFDM, which effects the BER performance at low matrix dimensions.

E. Effect of the Matrix Dimensions on the BER of RSC-URC coded OFDM, AFDM, and OTFS

The BERs of RSC-URC-coded BPSK AFDM 1 and 2, OFDM, and OTFS 1, 2 and 3 are shown in Figure 8 for $R_c=0.9$ and $It_{inner}=2$ and $It_{outer}=8$ iterations, for the variable values of Set 1, 2, 3 and 4. When the Set index is reduced, the dimension of the system configurations is increased. As the matrix dimensions are increased, the BER trends of the AFDM and OTFS configurations converge, since the effect of the matrix dimensions is diminished.

F. E_b/N_0 gain of RSC-URC Coding Relative to Uncoded Transmission

The E_b/N_0 gains of Set 4 RSC-URC-coded BPSK AFDM 1 and 2, OFDM, and OTFS 1 and 2 relative to uncoded transmission for $R_c=0.5$ to 0.9 and $It_{inner}=2$ and $It_{outer}=8$ iterations at a BER of 10^{-3} is shown in Figure 9. The effective throughput in Bits Per Channel Use (bpcu) for each code rate is also shown. As expected, the E_b/N_0 gain reduces as the coding rate increases, since fewer errors can be corrected at higher coding rates. The E_b/N_0 gain is largest for the configurations with the worst uncoded BER performance, as the coding allows the OTFS and OFDM configurations to overcome the higher diversity gain of AFDM.

VI. Conclusions

Iterative soft-MMSE equalisation in conjunction with both RSC and RSC-URC coding has been conceived for AFDM, and both the BER and EXIT chart performance have been compared to that of OFDM and different OTFS configu-

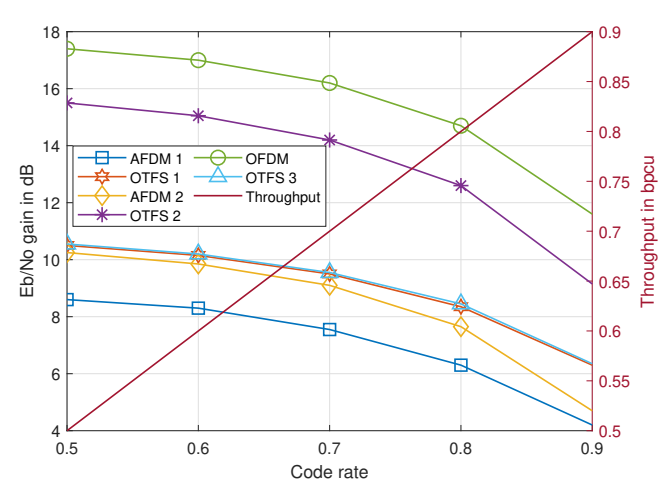


FIGURE 9: $\rm E_b/N_0$ gains of Set 4 RSC-URC-coded BPSK AFDM 1 and 2, OFDM, and OTFS 1 and 2 relative to uncoded transmission for $R_c=0.5$ to 0.9 and $\rm It_{inner}=2$ and $\rm It_{outer}=8$ iterations at a BER of 10^{-3}

rations. The results recorded for $R_c = 0.9$ and different variable Sets are summarised in Table 5. The AFDM configurations are shown to exhibit a lower BER at high E_b/N₀ than their equivalent OTFS counterparts, at lower matrix dimension, at high coding rates, and at low iteration number. This is because AFDM possesses higher degrees of freedom than OTFS, since AFDM is a one-dimensional waveform, whereas OTFS is two-dimensional. When the number of iterations is increased, the BER performance of the AFDM configurations and their equivalent OTFS configurations are shown to be similar. At the communication receiver velocity considered (150 m/s), both AFDM and OTFS tend to outperform OFDM, for both coded and uncoded transmission. Given that the RSC BER performance fails to improve beyond two iterations, this solution is recommended for lowcomplexity transceivers. By contrast, if the extra complexity of the RSC-URC aided transceiver is affordable, an extra E_b/N_0 gain of 1.8 dB may be attained at a BER of 10^{-5} and a code rate of 0.5.

Future work will investigate the relative performance of AFDM and OTFS for other coding methods, as well as for ISAC [25]–[33]. Other research areas of interest for coded AFDM are satellite communication [8], [43], [44], reconfigurable intelligent surfaces [38], [45], [46], and reconfigurable holographic surfaces [47].

REFERENCES

- [1] A. Bemani, N. Ksairi, and M. Kountouris, "AFDM: A Full Diversity Next Generation Waveform for High Mobility Communications," in 2021 IEEE International Conference on Communications Workshops (ICC Workshops), 2021, pp. 1–6.
- [2] T. Erseghe, N. Laurenti, and V. Cellini, "A multicarrier architecture based upon the affine Fourier transform," *IEEE Transactions on Communications*, vol. 53, no. 5, pp. 853–862, 2005.
- [3] X. Ouyang and J. Zhao, "Orthogonal Chirp Division Multiplexing," IEEE Transactions on Communications, vol. 64, no. 9, pp. 3946–3957,

2016

- [4] M. S. Omar and X. Ma, "Performance Analysis of OCDM for Wireless Communications," *IEEE Transactions on Wireless Communications*, vol. 20, no. 7, pp. 4032–4043, 2021.
- [5] R. Hadani, S. Rakib, M. Tsatsanis, A. Monk, A. J. Goldsmith, A. F. Molisch, and R. Calderbank, "Orthogonal Time Frequency Space Modulation," in 2017 IEEE Wireless Communications and Networking Conference (WCNC), 2017, pp. 1–6.
- [6] R. Hadani and A. Monk, "OTFS: A New Generation of Modulation Addressing the Challenges of 5G," 2018. [Online]. Available: https://arxiv.org/abs/1802.02623
- [7] Q. Li, J. Li, M. Wen, X. Dang, H. Arslan, and N. Al-Dhahir, "Affine Frequency Division Multiplexing for 6G Networks: Fundamentals, Opportunities, and Challenges," *IEEE Network*, pp. 1–1, 2025.
- [8] Y. Wang, Y. He, L. Zhao, and Y. Jiang, "AFDM Based Preamble Sequence Transmission for 6G Mobile Satellite Communication Systems," *IEEE Transactions on Wireless Communications*, pp. 1–1, 2025.
- [9] H. S. Rou and G. T. F. de Abreu, "Chirp-Permuted AFDM for Quantum-Resilient Physical-Layer Secure Communications," *IEEE Wireless Communications Letters*, pp. 1–1, 2025.
- [10] Y. I. Tek and E. Basar, "A Novel and Secure AFDM System for High Mobility Environments," *IEEE Transactions on Vehicular Technology*, pp. 1–6, 2025.
- [11] V. Savaux, "Special Cases of DFT-Based Modulation and Demodulation for Affine Frequency Division Multiplexing," *IEEE Transactions* on Communications, vol. 72, no. 12, pp. 7627–7638, 2024.
- [12] A. Bemani, G. Cuozzo, N. Ksairi, and M. Kountouris, "Affine Frequency Division Multiplexing for Next-Generation Wireless Networks," in 2021 17th International Symposium on Wireless Communication Systems (ISWCS), 2021, pp. 1–6.
- [13] A. Bemani, N. Ksairi, and M. Kountouris, "Affine Frequency Division Multiplexing for Next Generation Wireless Communications," *IEEE Transactions on Wireless Communications*, vol. 22, no. 11, pp. 8214–8229, 2023.
- [14] H. Yin, X. Wei, Y. Tang, and K. Yang, "Diagonally Reconstructed Channel Estimation for MIMO-AFDM With Inter-Doppler Interference in Doubly Selective Channels," *IEEE Transactions on Wireless Communications*, vol. 23, no. 10, pp. 14066–14079, 2024.
- [15] K. Zheng, M. Wen, T. Mao, L. Xiao, and Z. Wang, "Channel Estimation for AFDM With Superimposed Pilots," *IEEE Transactions* on Vehicular Technology, vol. 74, no. 2, pp. 3389–3394, 2025.
- [16] H. Xia, A. Zhang, D. Guo, D. Tian, and S. Wang, "A Single-Pilot-Aided Channel Estimation Scheme Based on Interference Position Indices for AFDM in Delay-Doppler Channels," *IEEE Wireless Communications Letters*, pp. 1–1, 2025.
- [17] H. Yuan, Y. Xu, X. Guo, Y. Ge, T. Ma, H. Li, D. He, and W. Zhang, "PAPR Reduction With Pre-Chirp Selection for Affine Frequency Division Multiplexing," *IEEE Wireless Communications Letters*, vol. 14, no. 3, pp. 736–740, 2025.
- [18] V. M. Reddy and H. Bitra, "PAPR in AFDM: Upper Bound and Reduction with Normalized mu-Law Companding," *IEEE Access*, pp. 1–1, 2025.
- [19] J. Zhu, Q. Luo, G. Chen, P. Xiao, and L. Xiao, "Design and Performance Analysis of Index Modulation Empowered AFDM System," *IEEE Wireless Communications Letters*, vol. 13, no. 3, pp. 686–690, 2024.
- [20] Y. Tao, M. Wen, Y. Ge, J. Li, E. Basar, and N. Al-Dhahir, "Affine Frequency Division Multiplexing With Index Modulation: Full Diversity Condition, Performance Analysis, and Low-Complexity Detection," *IEEE Journal on Selected Areas in Communications*, vol. 43, no. 4, pp. 1041–1055, 2025.
- [21] G. Liu, T. Mao, Z. Xiao, M. Wen, R. Liu, J. Zhao, E. Basar, Z. Wang, and S. Chen, "Pre-Chirp-Domain Index Modulation for Full-Diversity Affine Frequency Division Multiplexing towards 6G," *IEEE Transactions on Wireless Communications*, pp. 1–1, 2025.
- [22] M. Qian, F. Ji, Y. Ge, M. Wen, and Y. L. Guan, "Index modulated affine frequency division multiplexing with spread spectrum," 2025. [Online]. Available: https://arxiv.org/abs/2505.09394
- [23] X. Wang, L. Xiao, Q. Luo, J. Zhou, M. Wen, and T. Jiang, "Low-complexity Vector-by-Vector Detector for AFDM-IM Systems by Reconstructing Sparse Channel Matrix," *IEEE Communications Letters*, pp. 1–1, 2025.
- [24] Q. Luo, P. Xiao, Z. Liu, Z. Wan, N. Thomos, Z. Gao, and Z. He, "AFDM-SCMA: A Promising Waveform for Massive Connectivity

- Over High Mobility Channels," *IEEE Transactions on Wireless Communications*, vol. 23, no. 10, pp. 14421–14436, 2024.
- [25] H. S. Rou, G. T. F. de Abreu, J. Choi, D. González G., M. Kountouris, Y. L. Guan, and O. Gonsa, "From Orthogonal Time–Frequency Space to Affine Frequency-Division Multiplexing: A comparative study of next-generation waveforms for integrated sensing and communications in doubly dispersive channels," *IEEE Signal Processing Magazine*, vol. 41, no. 5, pp. 71–86, 2024.
- [26] Y. Ni, Z. Wang, P. Yuan, and Q. Huang, "An AFDM-Based Integrated Sensing and Communications," in 2022 International Symposium on Wireless Communication Systems (ISWCS), 2022, pp. 1–6.
- [27] A. Bemani, N. Ksairi, and M. Kountouris, "Integrated Sensing and Communications With Affine Frequency Division Multiplexing," *IEEE Wireless Communications Letters*, vol. 13, no. 5, pp. 1255–1259, 2024.
- [28] Y. Ni, P. Yuan, Q. Huang, F. Liu, and Z. Wang, "An Integrated Sensing and Communications System Based on Affine Frequency Division Multiplexing," *IEEE Transactions on Wireless Communications*, vol. 24, no. 5, pp. 3763–3779, 2025.
- [29] K. R. R. Ranasinghe, H. Seok Rou, G. Thadeu Freitas de Abreu, T. Takahashi, and K. Ito, "Joint Channel, Data, and Radar Parameter Estimation for AFDM Systems in Doubly-Dispersive Channels," *IEEE Transactions on Wireless Communications*, vol. 24, no. 2, pp. 1602–1619, 2025.
- [30] F. Xiao, Z. Li, and D. Slock, "Multipath Component Power Delay Profile Based Joint Range and Doppler Estimation for AFDM-ISAC Systems," 2025. [Online]. Available: https://arxiv.org/abs/2503.10833
- [31] F. Zhang, Z. Wang, T. Mao, T. Jiao, Y. Zhuo, M. Wen, W. Xiang, S. Chen, and G. K. Karagiannidis, "AFDM-Enabled Integrated Sensing and Communication: Theoretical Framework and Pilot Design," 2025. [Online]. Available: https://arxiv.org/abs/2502.14203
- [32] J. Zhu, Y. Tang, F. Liu, X. Zhang, H. Yin, and Y. Zhou, "AFDM-Based Bistatic Integrated Sensing and Communication in Static Scatterer Environments," *IEEE Wireless Communications Letters*, vol. 13, no. 8, pp. 2245–2249, 2024.
- pp. 2245–2249, 2024.
 [33] Y. Luo, Y. L. Guan, Y. Ge, D. González G, and C. Yuen, "A Novel Angle-Delay-Doppler Estimation Scheme for AFDM-ISAC System in Mixed Near-Field and Far-Field Scenarios," *IEEE Internet of Things Journal*, vol. 12, no. 13, pp. 22 669–22 682, 2025.
 [34] C. Sturm and W. Wiesbeck, "Waveform Design and Signal Processing
- [34] C. Sturm and W. Wiesbeck, "Waveform Design and Signal Processing Aspects for Fusion of Wireless Communications and Radar Sensing," Proceedings of the IEEE, vol. 99, no. 7, pp. 1236–1259, 2011.
- [35] Z. Li, C. Zhang, G. Song, X. Fang, X. Sha, and D. Slock, "Chirp Parameter Selection for Affine Frequency Division Multiplexing with MMSE Equalization," *IEEE Transactions on Communications*, pp. 1– 1, 2024.
- [36] X. Li, H. Wang, Y. Ge, X. Shen, Y. L. Guan, M. Wen, and C. Yuen, "Affine Frequency Division Multiplexing Over Wideband Doubly-Dispersive Channels With Time-Scaling Effects," *IEEE Transactions* on Wireless Communications, pp. 1–1, 2025.
- [37] J. Xu, Z. Liang, and K. Niu, "Multi-Block UAMP Detection for AFDM Under Fractional Delay-Doppler Channel," in 2025 IEEE Wireless Communications and Networking Conference (WCNC), 2025, pp. 1–6.
- [38] C. Xu, L. Xiang, J. An, C. Dong, S. Sugiura, R. G. Maunder, L.-L. Yang, and L. Hanzo, "OTFS-Aided RIS-Assisted SAGIN Systems Outperform Their OFDM Counterparts in Doubly Selective High-Doppler Scenarios," *IEEE Internet of Things Journal*, vol. 10, no. 1, pp. 682–703, 2023.
- [39] C. Xu, S. Sugiura, S. X. Ng, P. Zhang, L. Wang, and L. Hanzo, "Two Decades of MIMO Design Tradeoffs and Reduced-Complexity MIMO Detection in Near-Capacity Systems," *IEEE Access*, vol. 5, pp. 18564– 18632, 2017.
- [40] C. Xu, D. Liang, S. Sugiura, S. X. Ng, and L. Hanzo, "Reduced-Complexity Approx-Log-MAP and Max-Log-MAP Soft PSK/QAM Detection Algorithms," *IEEE Transactions on Communications*, vol. 61, no. 4, pp. 1415–1425, 2013.
- [41] P. Robertson, E. Villebrun, and P. Hoeher, "A comparison of optimal and sub-optimal MAP decoding algorithms operating in the log domain," in *Proceedings IEEE International Conference on Commu*nications ICC '95, vol. 2, 1995, pp. 1009–1013 vol.2.
- [42] L. Hanzo, T. H. Liew, B. L. Yeap, R. Y. S. Tee, and S. X. Ng, Turbo Equalisation for Partialresponse Systems, 2011, pp. 289–323.
- [43] X. Qiang, L. You, C. G. Tsinos, W. Wang, X. Gao, and B. Ottersten, "Joint Communications and Sensing for Hybrid Massive MIMO LEO Satellite Systems With Beam Squint," in 2022 IEEE International

- Conference on Communications Workshops (ICC Workshops), 2022, pp. 963–968.
- [44] S. Aliaga, A. J. Alqaraghuli, and J. M. Jornet, "Joint Terahertz Communication and Atmospheric Sensing in Low Earth Orbit Satellite Networks: Physical Layer Design," in 2022 IEEE 23rd International Symposium on a World of Wireless, Mobile and Multimedia Networks (WoWMoM), 2022, pp. 457–463.
- [45] C. Xu, J. An, T. Bai, L. Xiang, S. Sugiura, R. G. Maunder, L.-L. Yang, and L. Hanzo, "Reconfigurable Intelligent Surface Assisted Multi-Carrier Wireless Systems for Doubly Selective High-Mobility Ricean Channels," *IEEE Transactions on Vehicular Technology*, vol. 71, no. 4, pp. 4023–4041, 2022.
- [46] C. Pan, H. Ren, K. Wang, J. F. Kolb, M. Elkashlan, M. Chen, M. Di Renzo, Y. Hao, J. Wang, A. L. Swindlehurst, X. You, and L. Hanzo, "Reconfigurable Intelligent Surfaces for 6G Systems: Principles, Applications, and Research Directions," *IEEE Communications Magazine*, vol. 59, no. 6, pp. 14–20, 2021.
- [47] R. Deng, Y. Zhang, H. Zhang, B. Di, H. Zhang, and L. Song, "Reconfigurable Holographic Surface: A New Paradigm to Implement Holographic Radio," *IEEE Vehicular Technology Magazine*, vol. 18, no. 1, pp. 20–28, 2023.



Hugo Hawkins (Graduate Student Member, IEEE) received his B.Eng. degree in Electrical and Electronic Engineering from the University of Southampton with First Class Honours in 2021. He is currently undertaking a PhD within the Next Generation Wireless Research Group at the University of Southampton. His research interests include integrated sensing and communication.



Chao Xu (Senior Member, IEEE) is a Senior Lecturer with Next Generation Wireless Research Group, University of Southampton. His research interests include integrated sensing and communication, optical wireless, and quantum key distribution. He was the recipient of the 2023 Marie Sklodowska-Curie Actions Global Postdoctoral Fellowships with the highest evaluation score of 100/100.



Lie-Liang Yang (Fellow, IEEE) is the professor of Wireless Communications at the University of Southampton, UK. He has research interest in wireless communications, wireless networks and signal processing for wireless communications, as well as molecular communications and nanonetworks, with 400+ research papers and 4 books. He is also a fellow of IET, AAIA and AIIA.



LAJOS HANZO (Life Fellow, IEEE) Lajos Hanzo (FIEEE'04) received Honorary Doctorates from the Technical University of Budapest (2009) and Edinburgh University (2015). He is a Foreign Member of the Hungarian Science-Academy, Fellow of the Royal Academy of Engineering (FREng), of the IET, of EURASIP and holds the IEEE Eric Sumner Technical Field Award. For further details please see http://www-mobile.ecs.soton.ac.uk, https://en.wikipedia.org/wiki/Lajos_Hanzo